Photon-echo-based Optical Data Compression Using an External Cavity Diode Laser

Master's Thesis By
Xiangjun Wang

LRAP-250, Lund, Dec. 1999

Supervised By
Prof. Stefan Kröll

Table of Contents

Abstract

Single pulse compression and multi-bit pulse compression using the photon echo process was investigated. A single pulse could be compressed by a factor of 454 from 10 microseconds to 22 nanoseconds. A 10-bits pulse train was compressed by a factor of 92 from 20 microseconds in total length to 212 nanoseconds. The compression factors obtained during this work were an order of magnitude better than those published previously both for single pulse and multi-bit pulse train compression. Observation of the side-band under the envelope of the photon echo signal in multi-bit pulse compression indicates that the bit information is retained in the compression. Some improvements were achieved by optimising the experimental setup during the work. The experimental results were discussed theoretically and were good in agreement with theoretical calculations. The space-time duality of photon echo compression was also analysed in this thesis.

The storage material used in the experiment is a YAG crystal doped with the trivalent rare earth thulium ion with a concentration at 0.1-at. %. The crystal was kept at 4K during the experiment. The absorption, an important characteristic of the crystal was initially measured. The maximum absorption was about 40%, in the range between 7931.50 Å and 7931.60 Å with a full width of half maximum of 3.5 Å, which corresponds to 19 GHz.

A homemade external cavity diode laser equipped with an intra- high coherency and ultrahigh-speed frequency chirping properties was used in the experiments. This system with an intra-cavity electro-optic crystal (EOC) was employed for the optical data compression because of its advantages of simplicity, high quantum efficiency, low cost, and compact size, which is necessary for practical applications in the future. Some critical properties for this laser were investigated. The laser line-width was measured to be 350 KHz over a 200 microseconds duration using the spectral hole burning method and a voltage-chirping rate of about 7 MHz/V was determined by calculations and experimental measurements.

1. Introduction

1. 1 General introduction

Optical data storage by spectral hole burning and photon echo techniques have attracted interest from researchers for many years because of its predicted high storage density (10^{11} to 10^{15} bits/cm^2) and its large potential for practical applications. To get an impression of what these storage densities actually mean we note that 1 Tbit/cm^2 ($1.25\text{x}10^{11}$Bytes/cm^2) correspond to $4.2\text{x}10^7$ pages of ascii text, $1.25\text{x}10^5$ pages of color images, $1.25\text{x}10^4$ min. (8.7 days) of CD audio recording or $4.2\text{x}10^3$ min. (2.89 days) of video film [7]. A temporal optical data sequence that consists of data information can be written into a storage medium as it propagates through the storage medium using photon echo technique.

Among the all-optical capabilities that have been demonstrated with photon echoes are storage of 4000 bits of data at a single spatial location [24], recognition of temporal data [5], high-speed image processing [6], realisation of a complete ser of Boolean operators [20,21] projected storage densities of the order of Tbits/cm^2 and THz data rates, experimental demonstration of storage and recall of data at THz rates [22,23], pulse compression, data rate conversion [8,10], spatial routing and selection of beams based on their temporal information contents [12,19] and amplifying photon echoes with a fiber amplifier [16]. Most of these demonstrations have been performed in rare-earth-ion-doped inorganic crystals. With the closely related persistent spectral hole-burning technique, storage of 6000 holograms, each containing 400 bits has been demonstrated in a spatial area of 6 cm^2 [17]. Recording a continuous "movie" of a 20 seconds long event in real time and replaying it at an arbitrary speed, has also been demonstrated at a single spatial location [18].

1.2 Objective of the diploma work

As mentioned above transient coherent data rate conversion and bit-stream reversal is one of the current frontier topics in the photon optical data storage and processing field. Using the photon echo technique a pulse form which constitute of a single pulse or a multi-bit pulse train can be compressed in time by an interaction with a second pulse in a storage medium when the frequency chirping speed over the second pulse is twice as fast as that of the data pulse sequence. On the other hand a dense data pulse sequence can also be expanded using a scheme similar to that required for the compression. In theory a few or a few tens of microseconds long pulse can be compressed by factor of 1000 to 10000 times with the equipment used in this experiment. The limit set by the best photon echo materials would be compression by a factor 10^8. The limitation on the compression ratio that can be obtained in the present experiment is due to the limited frequency chirping interval and the limited stability of the laser system. It should be readily possibly to apply the procedure demonstrated in this thesis to other time scales. For example a few or a few tens of nanoseconds long pulse can reasonably be compressed by factor in the same order of magnitude to a few picoseconds.

Previously single pulse compression by a factor of 10 using dye lasers has been demonstrated in our group. This is also roughly the extent to which other groups have compressed pulses using photon echoes [8,9,10]. However, the diode laser system is very attractive to use for optical data storage especially for optical data conversion and bit-stream reversal since its output beam frequency can easily be linearly chirped with ultrahigh speed over very large

intervals. It also has other advantages, for example, wavelength tunability, compactness, simplicity, and low cost. It was anticipated that a homemade external cavity diode laser [3] equipped with an intra-cavity electro-optic crystal (EOC) would enable me to get a better compression factor than previously has been obtained.

The objectives of the diploma work were mainly:
1. To learn how to operate and control the diode laser wavelength and single mode power by altering the temperature, operating currents and length of the diode laser cavity and how to handle eletro-, optoelectronics to modulate the amplitude and frequency of the laser beam.
2. To determine the frequency stability of the diode laser system by spectral hole-burning method as well as characterize other properties of the laser system.
3. Experiment on single pulse compression and multi-bit pulse train compression by photon echoes. Investigate the characteristics of data compression by analysing photon echo data. Analysing the practical limitations to the experimental result and compare with the theoretical predictions in order to identify the improvements needed for obtaining still better compression.

2. Theoretical description of coherent transient optical data compression

2.1 Physical description of the photon echo process

This section essentially follows the description given in Ref. 13. We assume that a two-level system is irradiated by two temporally separated excitation pulses. Atoms resonant with the first excitation pulse are excited to the upper lever, and the system then possesses an oscillating, macroscopic, electric dipole moment. This dipole moment will dephase as a function of time. At time t the second temporal excitation pulse comes in and causes the dipole moment to begin to rephase. At time 2t the rephasing is completed and the system emits a photon echo signal.

This concept also can be described using conventional quantum mechanics. Again assuming a two-level system with energy E_g, and E_e of the upper and lower state, respectively. The wave functions of these are represented by

$$\psi_g = \phi_g \exp(-iE_g t/\hbar) \tag{2.1}$$

$$\psi_e = \phi_e \exp(-iE_e t/\hbar) \tag{2.2}$$

Where $\emptyset_g$ and $\emptyset_e$, are the eigen wave function of the ground and excited states, respectively. The wave function of the total system then can be given by

$$\psi_{total} = a\psi_g + b\psi_e \tag{2.3}$$

where $|a|^2 + |b|^2 = 1$. Now the charge distribution can be expressed as

$$\rho_e = -e\left|\psi_{total}\right|^2 \propto \mathrm{Re}(\psi_g \psi_e^*) + \text{other terms} \tag{2.4}$$

The real part of the first term in equation (2.4) can be described by

$$\mathrm{Re}\left[\left(\phi_g \phi_e^*\right)\exp\left(i\left(E_e - E_g\right)t/\hbar\right)\right] \tag{2.5}$$

The polarisation is proportional the first term in the equation (2.5), so that it can be descried as [7]

$$P \propto \cos\left[\left(\omega_e - \omega_g\right)t\right] \tag{2.6}$$

From classical electro-magnetic field theory an oscillation charge distribution or a microscopic oscillating polarisation will generate an electro-magnetic field. Thus atoms in a superposition of two states should radiate.

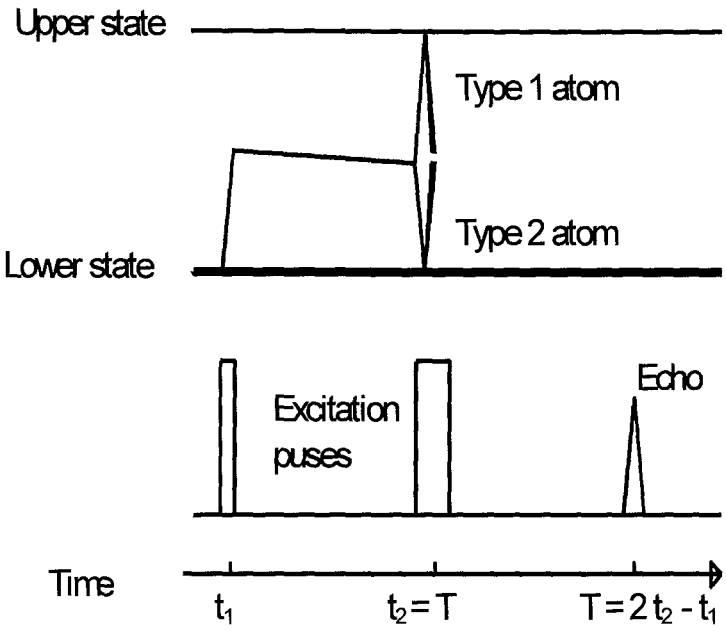

Figure 2.1 Illustration on photon echo generation

From the description above it is reasonable to imagine that atoms in a superposition of states radiate and that this radiation interfere with any other radiation. The relative phase of radiation emitted by the atoms and any incoming radiation will determine whether the system will undergo absorption or stimulated emission. If the radiation sent out from the atoms is in phase with the incoming radiation. The radiation will be stronger after the pulse passed the atom. On the contrary, if the phase of the radiation sent out from the atoms is opposite to the phase of incoming radiation, the radiation intensity will be smaller after passing the atoms.

An alternative view of the process of two pulses interaction with atoms that maintain their phase coherence is given in Figure 2.1. On the horizontal axis we have time. The excitation pulses are displayed in the lower part of the figure. In the upper part two horizontal lines representing the ground state and the excited state are shown. The curve evolving in time between these two states shows the probability to find the atoms in the upper state. As the first pulse arrives the probability to find the atoms in the upper state starts to rise from zero to about 50% when the first pulse ends. It is assumed that the lifetime of the excited state is much longer than the separation between the pulses. The probability for the atoms to be in the upper state therefore only decreases a little between the first and second pulse. As the second pulse enters the in-phase atoms will be de-excited and the out-of-phase atoms will be excited. Following Figure 2.1 "Type 1" atoms are in the excited state and "Type 2" atoms are in the ground state. The "Type 1" atoms are, according to Figure 2.1, all excited. Their further interaction with the radiation can therefore only result in that they are de-excited, i.e. simulated emission. They will therefore start to radiate in phase with the excitation pulse. The "Type 2" atoms are in the ground state and must interact by absorbing light. They will therefore start to radiate out of phase with the excitation pulse. The excitation process is then continued until the atoms, as after the first pulse, are in a superposition of the ground and excited state. However, now the situation is different than after the first pulse. Because when the first pulse was turned off all

atoms were oscillating in phase, but now, after the second pulse, the "Type 1" and "Type 2" atoms are 180 degrees out of phase. This means that, contrary to what was the case at time t = T both type 1 and type 2 atoms oscillate in phase at time 2T and a strong pulse will be radiated by the sample.

This is the two-pulse photon echo. A coherent emission, the photon echo, occurs at time $t = t_2 + (t_2 - t_1)$. There is also some coherent emission right after the excitation pulse since at these times many atoms also radiate in phase. The coherent emission gradually fading away after each pulse is called the "free induction decay" (FID) [13].

2.2 Fourier-transform description of photon echo optical data compression

It is predicted that linearly chirped optical pulses can give rise to photon echoes whose minimum duration is limited only by the total material bandwidth that contributes to the echo signal [9,10]. The photon echo process acts as a frequency-dependent optical delay line whose dispersion is determined by the chirp rate of the excitation pulses rather than by their bandwidth. Consequently, long and short pulses can be compressed with equivalent techniques without complicated alignment procedure.

2.2.1 Single pulse compression

Using two successive linearly chirped pulses that resonantly interact with an inhomogeneously broadened material to generate a photon-echo performs single pulse compression. In principle, quite long chirped pulses can be compressed using this method. Consider a strongly inhomogenerously broadened sample of two-level atoms that is irradiated by two resonant excitation pulses. The electromagnetic fields of the first pulse and of the second pulse are denoted E_1 and E_2, respectively. The echo output field as a function of time, $E_e(t)$, equals the first input field $E_1(t)$ correlated with the second field $E_2(t)$ convoluted with itself i.e. which is referred from [10],

$$E_e(t) \propto \int_{-\infty}^{\infty} E_1^*(\omega) E_2^2(\omega) \exp(i\omega t) d\omega \qquad (2.7)$$

where $E_i(\omega)$ is the frequency Fourier transform of $E_i(t)$. We consider two chirped excitation pulses, of lengths $T_1 = T$ and $T_2 = T/2$ as in Fig 2.2. Assume that both excitation pulses are chirped over the bandwidth $\omega_{ch} T >> 1$. Within the time interval $t \in [t_i - T_i/2, t_i + T_i/2]$ we write the electric field of pulse i as $E_i(t) = \exp\{\{-i[\omega_0 + K(t-t_1)](t-t_i)\}\exp-(i\vec{k}_i \bullet \vec{r})$, where the echo will now appear in the direction $k_e = 2\vec{k}_2 - \vec{k}_1$ at time $t_e = 2t_2 - t_1$. Graf *et al.* [10] suggested that, in the regime $\omega_{ch} T >> 1$, the excitation pulses can be regarded as constant in the frequency interval $[\omega_0 - \omega_{ch}/2, \omega_0 + \omega_{ch}/2]$ and zero othervise. Relation (2.7) can then be simplified as

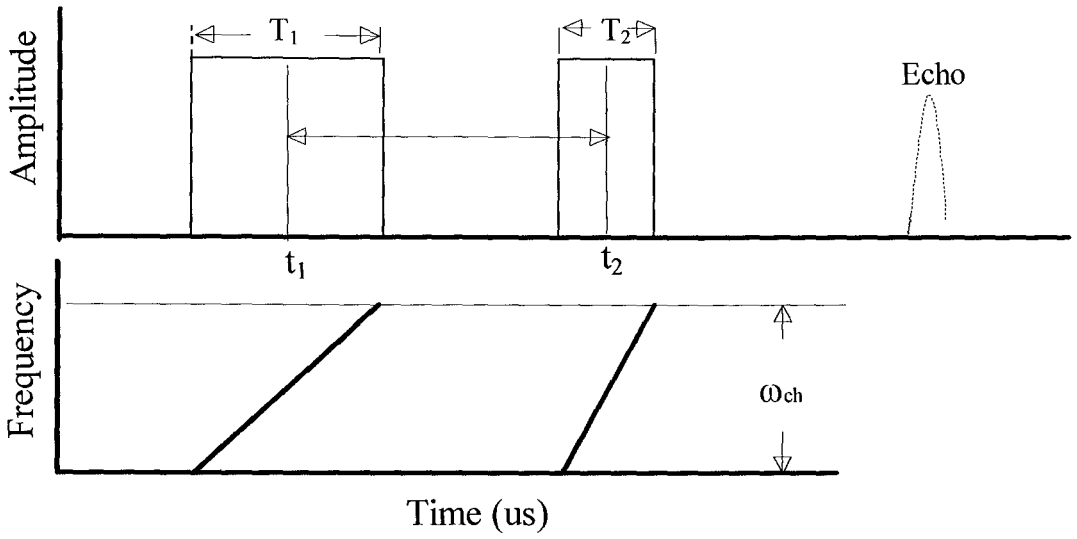

Figure 2.2 Amplitude and frequency sequence on single pulse compression

$$E_e(t) \propto \int_{\omega_0-\omega_{ch}/2}^{\omega_0+\omega_{ch}/2} \exp(i\omega t)d\omega = \exp(i\omega_0 t)\omega_{ch} \times \mathrm{sinc}\left(\frac{\omega_{ch}}{2}t\right), \qquad (2.8)$$

where we now have chosen zero for the time axis such that the echo occurs at time $t_e = 0$. The intensity of the echo will be proportional to

$$I_e \propto |E_e(t)|^2 \propto {\omega_{ch}}^2 \sin c^2 \frac{\omega_{ch}}{2}t \qquad (2.9)$$

The full width at half-maximum (FWHM) for the intensity of this echo pulse is approximately $T_e = 5.5/\omega_{ch}$,(2.10).

2.2.2 Multi-bit pulse train compression

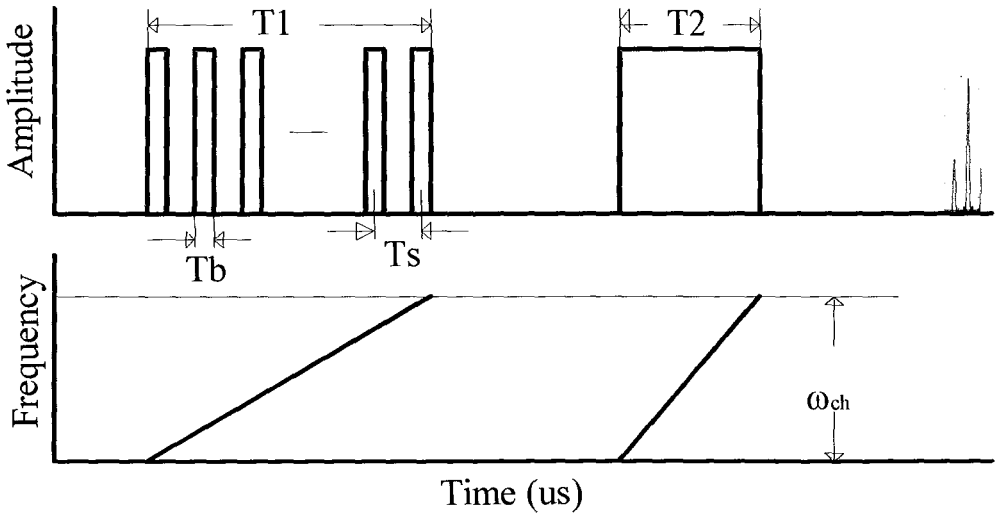

Figure 2.3 Amplitude and frequency sequence for a multi-bit pulse train compression

The results obtained from section 2.2.1 can now be used to analyse multi-bit pulse compression. As shown in Figure 2.3 a multi-bit pulse train with total length of T_1 is compressed by the interaction with the second pulse with length of $T_2 = T_1/2$. Each bit has duration of T_b, the center-center separation between the bits is T_S and the chirping speed of the second pulse is twice as fast as that during the pulse train. If only $\omega_{ch}T_b >> 1$, the echoes of the separate bits will all appear at the sane time. To get the resultant echo field it is then sufficient to sum the echo fields from all the individual bits. (If $\omega_{ch}T_b << 1$ and $\omega_{ch}T >> 1$ the first pulse will work as a brief pulse and the echo will have duration T.) Summing the echo output field for several individual bits j in the relation (2.8), we obtain

$$E_{tot}(t) = \sum_j E_j(t) \propto {\omega_{ch}}^b \operatorname{sinc} {\omega_0}^j \left(\frac{{\omega_{ch}}^b}{2} t \right) \sum_j \exp\left(i{\omega_0}^j t\right) \qquad (2.11)$$

In our case all bits have the same duration and ${\omega_{ch}}^b$ is independent of j. ${\omega_0}^j$ is the center frequency of bit j and can be expressed as ${\omega_0}^j = \omega_0 + (\omega_{ch}/T)T_s(j-1)$, where ω_0 is the central frequency of the first bit $\left(\omega_0 = {\omega_0}^1\right)$. Relation (2.10) become particularly simple if the i.e., if j runs from 1 to N_b, where N_b is the number of bits in the sequence. The resultant intensity then becomes

$$I(t) \propto {\omega_{ch}}^{b2} \operatorname{sinc}^2\left(\frac{{\omega_{ch}}^b}{2} t \right) \frac{\sin^2\left(N_b \frac{{\omega_{ch}}^b}{2T_b} T_S t \right)}{\sin^2\left(\frac{{\omega_{ch}}^b}{2T_b} T_S t \right)} \qquad (2.12)$$

The duration of compressed multi-bit photon echo is the same as that of single pulse compression where the bit duration is T_b. That is, put T_b, ${\omega_{ch}}^b$ instead of ω_{ch} in the equation (2.10) and the bit duration then will be given as:

$$T_e \propto \frac{1}{{\omega_{ch}}^b} \propto \frac{T_1}{\omega_{ch} \cdot T_b} \qquad (2.13).$$

3. Experiment

3.1 Arrangement of experimental set-up

The experimental set-up is shown in Figure 3.1 in page 12. A homemade external cavity single model diode laser (D.L.) equipped with an intra-cavity electro-optic crystal (EOC) was tuned to the $^3H_4$ - $^3H_6$ transition line of the trivalent rare earth ion Tm^{3+} doped into YAG at 793.1 nm. The laser wavelength and the laser mode were monitored by a wavelength meter and a Coherent Model 240 Spectrum Analyzer, respectively. The laser frequency can easily be linearly chirped over large intervals by supplying a voltage ramp, generated from a Stanford Research, model DS345 30MHz Synthesized Function Generator and a New Focus 3211 High Voltage Amplifier, to the intra-cavity EOC. The laser output power is about 30 mW with a short time linewidth of about 350 kHz.

The acousto-optic modulator (AOM) system, which consists of Isomet Corporation, 1205C acousto-optic modulators (AOM1 and AOM2), is utilized to create pulses for single pulse compression. An additional HP 8013B pulse generator is added to the system for multi-bit pulse train compression. The excitation pulses were obtained as the pair of AOMs were simultaneously driven by a RF Generator and a high power amplifier.

A 0.1-at. % thulium-doped YAG crystal, 5 mm thick in the direction of light propagation, was submerged in the liquid helium contained in the CryoVac 3-11-2228 E cryostat, in which the temperature was kept at about 4°K.

The laser spot, about 2 mm in diameter, is focused onto the crystal by a 10-cm focal-length lens. The echo signal was detected with a Hamamatsu R943-02 photo-multiplier tube (PMT). Another Isomet Corporation 1205C acousto-optic modulator (AOM3) was inserted between the crystal and the PMT to reject the excitation pulses at the detection side.

The equipment used above will be described in details in the following sub-sections. In particular I will describe the acousto-optic modulator and the electro-optic crystal inside the laser for modulating the amplitude and frequency respectively, as well as structure of the laser and its properties.

3.2 Amplitude and frequency modulation

3.2.1 Amplitude modulation by using an acousto-optic modulator (AOM)

How do you modulate a continuous wave laser into an arbitrary pulse sequence? The general idea, to give a simple answer to the question, is to use some sort of mechanical method such as a shutter or a chopper wheel. The disadvantage of these sort of mechanical devices is that it is difficult to achieve a very high bit-rate as they have rather long rise and fall time and especially chopping wheels do not can change their sequence randomly, i.e., they are unable to vary the pulse duration and separation randomly. A modulator based on the acousto-optic effect can successfully meet these requirements though [14].

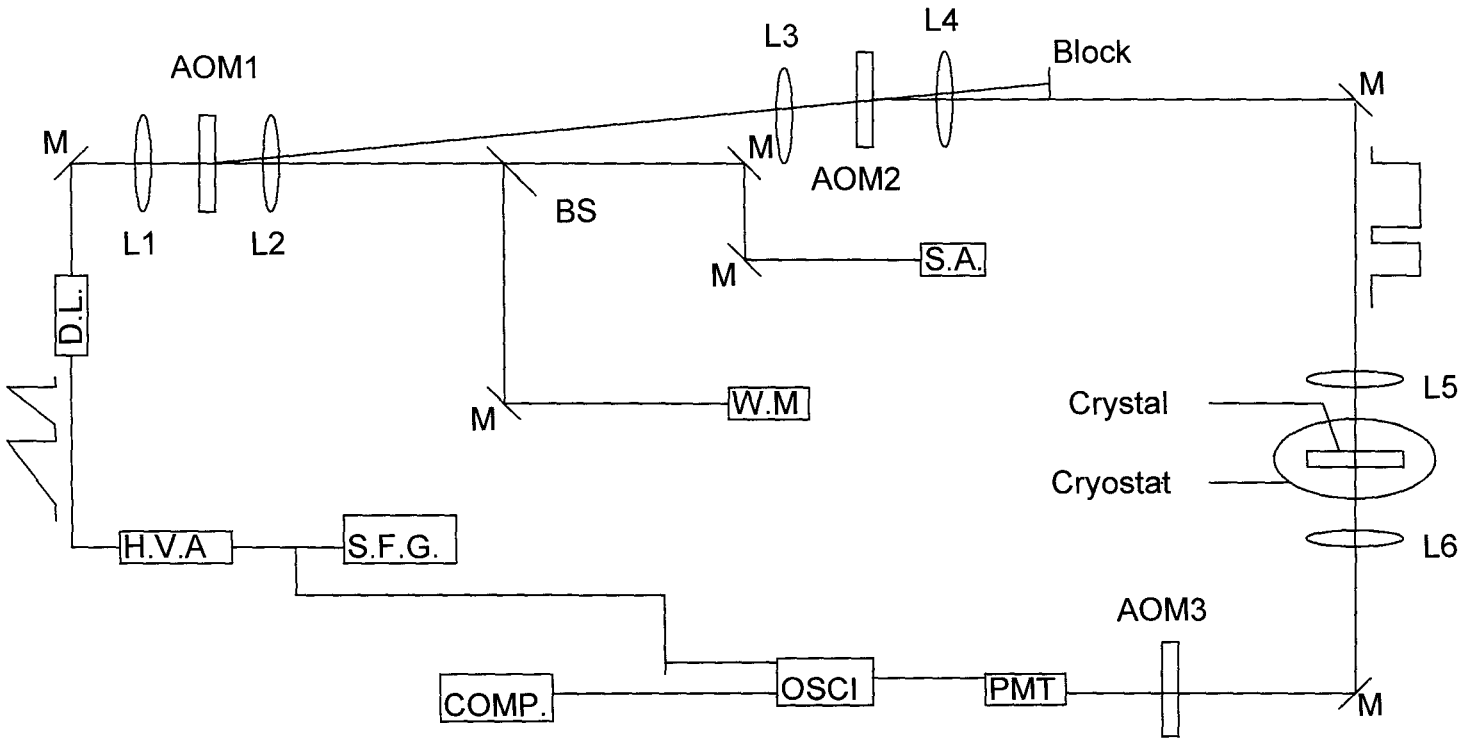

Figure 3.1 Experimental set-up. Abbreviations in the figure stand for the following,
D.L.: diode laser, M: mirror, AOM: acousto-optic modulator, W.M.: wavelength meter,
S.A.: spectral analyzer, H.V.A.: high voltage amplifier, S.F.G.: synthesized function generator,
PMT: photo-multiplier tube, OSCI: oscilloscope, COMP.: computer, BS: beam splitter and L: lenses.

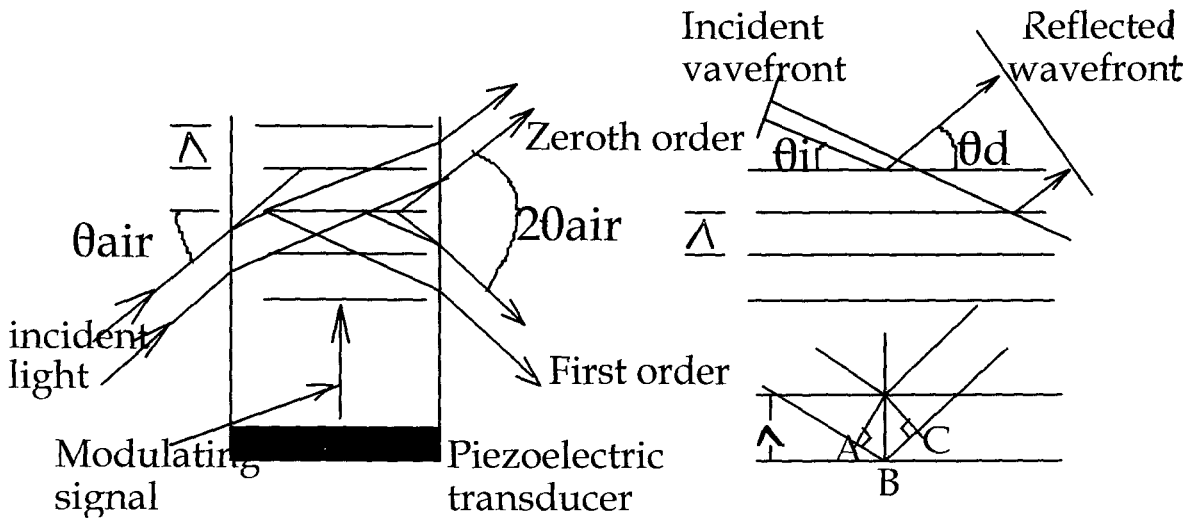

Figure 3.2 Illustration of an acousto-optic modulator with Bragg-reflection, The distance AB + BC corresponds to an integer number of wavelengths.

By applying a RF (radio frequency) power source on/off with the desirable sequence to an acousto-optic modulator (AOM), an acoustic wave is formed and spread through the AOM. Incident light will be diffracted when it hits the acoustic wave front. Consequently a diffracted beam with a sequence mirroring the RF power sequence can be obtained in a direction with a small angle relative to the direction of the incident light. This is illustrated in the figure 3.2.

The condition for high reflectivity is given by

$$\theta_i = \theta_d \Rightarrow \sin\theta_i = \sin\theta_d = m\lambda/2\Lambda \qquad (3.1)$$

Where Λ = speed of sound in the crystal divided by the frequency by which the piezoelectric transducer is modulated, (i.e. the sound wave length in the crystal,
λ = the light wavelength in the medium,
θ_i = incident angle to the medium,
θ_d = reflection angle at the medium.
m = integer number

Combining Snell's law $n \sin\theta_d = \sin\theta_{air}$, the $\sin\theta_{air}$ is given by

$$\sin\theta_{air} = m\lambda_0/2\Lambda \qquad (3.2)$$

where λ_0 = the light wavelength in the air.

The diffraction efficiency depends on the RF power.
In the experimental set-up a pair of AOMs were employed for creating the pulse sequences. The advantages of using a pair of AOMs instead a single AOM is that the light scattered into the direction of diffraction when the power is off can be reduced significantly so that the signal-to-background ratio can decrease from about 1% to 0.01%. The pair of AOMs operated by a RF power generator connected to a high power amplifier gives diffraction efficiencies about 45% and 40% at optimal RF output to

AOM1 and AOM2, respectively. It is important to adjust the AOMs accurately to get the highest diffraction efficiency, which in our experiment means to get the highest intensity in the first order diffraction. If a modulation voltage consisting of a pulse sequence is used for gating the RF output to the AOMs, then a diffraction beam with same sequence as the modulation voltage can be obtained when a continuous wave beam is diffracted by the acoustic wave on the AOMs.

3.2.2 Frequency modulation using an acousto-optic modulator (AOM) and the electro-optic crystal (EOM)

In the experiment both the acousto-optic modulator and the intra-cavity electro-optic modulator were employed for frequency modulation. Figure 3.2 again can illustrate the principle of the acousto-optic effect for frequency modulation. Light frequency will change as it goes through an AOM to which a RF frequency power is applied to the peizo crystal. The RF output frequency is linearly proportional to an input tuning voltage of the radio frequency driver. If a ramped tuning voltage is applied to the RF driver, the result will be that the light frequency changes linearly and proportionally to the tuning voltage. The relationship between the frequency, ω, of the incident light and the frequency, ω', of the diffraction light can be represented as [14]:

$$\omega' = \omega + c \cdot \Omega \qquad (3.3)$$

Where Ω stand for the frequency of the acoustic wave within the AOM and c is the diffraction order.

The other method for frequency modulation is based on the electro-optic effect. In electro-optic materials the refractive index is changed by the application of an electric field. In a birefringent crystal without an external electric field the index ellipsoid has the following form, which has been described at chapter 4 in Ref. 14:

$$\frac{x^2}{n_x^{\,2}} + \frac{y^2}{n_y^{\,2}} + \frac{z^2}{n_z^{\,2}} = 1 \qquad (3.4)$$

The change in reflective index is principally given by

$$\Delta\left(\frac{1}{n^2}\right) = rE + gE^2 \qquad (3.5)$$

Where E = applied field strength,
r = the linear electro-optic coefficient, leading to the Pockels effect,
g = the second-order electro-optic coefficient, leading to the Kerr effect.

In our case we consider the Pockels effect and the higher order term is usually negligible. So the refractive index change is linearly proportional to the external electric field. For the external cavity laser used here [3] the laser frequency can be linearly chirped by applying a voltage ramp to an intracavity electro-optic crystal. This causes the optical length of the laser cavity to change as the reflective index changes [3].

3.3 The external cavity diode laser

The use of diode lasers in physics research has expanded rapidly [4]. The key reasons are that diode lasers can provide frequency tunability, are inexpensive, easy to operate and of compact size. The special advantage of the diode laser system we used is that it can provide high-speed linear frequency chirps over large intervals at single-mode operation using an intra-cavity electro-optic crystal.

3.3.1 Structure of the diode laser system

The diode laser system was designed and made in our group in the year 1998. A schematic view of the homemade diode laser system is shown in Figure 3.3. A Littrow configuration was chosen mainly to minimise the external cavity length, but also to limit the sensitivity of the diode laser to vibrations. The output facet of the laser diode is antireflection coated. The EOC is a lithium tantalite crystal ($LiTaO_3$). Some parameters of the laser system are listed in Table 3.1. The total optical cavity length is about 4 centmeters. The components are mounted on a temperature controlled aluminium plate.

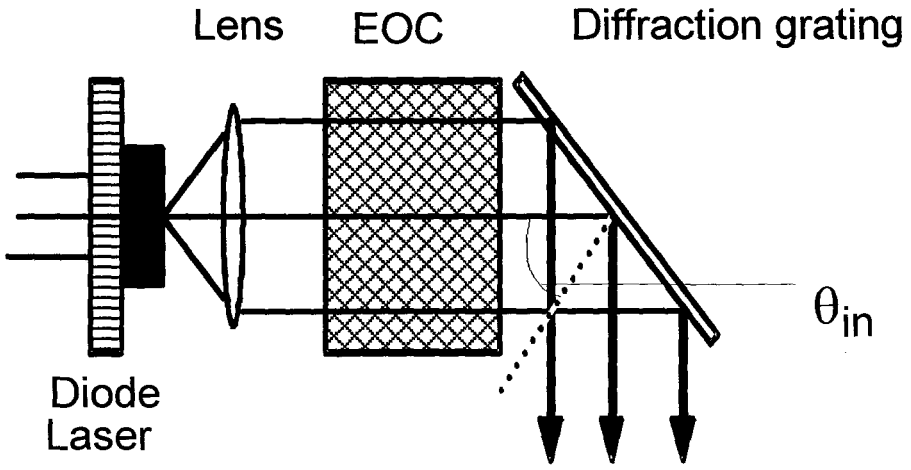

Figure 3.3 Schematic view of the diode laser system

Table 3.1 Parameters of the diode laser system [3]:

Diode laser:
AlGaAs/GaAs, Index guided quantum well structure,
At λ=800 nm, front facet R=10^{-5}, rear facet R=0.95,
Output power: 100mW.

Lens:
AR-coating R< 0.01,
N_A = 0.65, f = 2.75mm,
where N_A is the numeral aperture and f is the focal length of the lens.

Electro-optic crystal (EOC):
$LiTaO_3$ crystal (l_k,b_k,d_k = 5,4,1mm), r_{33} = 33x10^{-12} m/V, n_e = 2.16.

AR-coating R < 0.001
where l_k,b_k,d_k = dimension size in three axis of the EOC, r_{33} is a matrix element of tensor describing the linear electro optic effect and n_e is the refractive index along the direction of the applied electric field.

Grating:
1800 grooves/mm,
Diffraction efficiency, 24%-78% (depending on the polarization),
Diffraction angle, 45° at 800 nm

3.3.2 Properties of the diode laser system

The design above enable the diode laser system to be constructed with a small size, and single-mode wavelength tunability and the ability to linearly chirp the frequency with ultrahigh-speed over large intervals. Several important properties of the laser system will be described in the following sections:

1. Wavelength tunability
For any fixed cavity length there will be an infinite number of resonance frequencies. The frequency will change by changing the cavity length. Only the frequency closest to the maximum of the laser gain curve will lase. By adjustment of the cavity length the desired single-mode wavelength can be selected.

The temperature dependence of the wavelength occurs because the bandgap and the refractive index are altered with changing temperature.

The diode laser injection current can also influence the wavelength. This can also be explained by the thermal effect above.

In the diode laser system, wavelength tuning and single mode selection is achieved by a combination of cavity length adjustment, slightly rotating the grating and also by varying the temperature and the injection current of the diode laser. The wavelength change as a function of injection current is roughly 0.1-0.2 Å/mA. The wavelength change as a function of temperature is roughly 0.5-1.0 Å/°C. Mode jumps to an adjacent mode may occur when the temperature or injection current is changed. The maximum of the gain curve shifts by about 0.3Å/°C as a function of temperature.

2. Frequency chirping property
The EOC provides rapid voltage-controlled scans of the optical length of the cavity and hence output frequency tuning. The cavity length changes, dL, varies with the voltage, V, applied to the EOC according to the relation which was described in the Rene Nilsson's thesis [3] and [1,2].

$$dL = \lambda V / (2V_\pi) \qquad (3.4)$$

Where $V_\pi = \lambda d_k / (r_{33} n_e^3 l_k)$.

It follows that the laser output frequency varies, $d\gamma$, with applied voltage as

$$d\gamma = - \Delta\gamma_{ext} (V/ V_{\pi}) \qquad (3.5)$$

where Δ_{ext} represents external-cavity mode spacing.

The chirping-voltage rate can be given as

$$\frac{d\nu}{V} = - \frac{n_e^3 r_{33} l_k}{d_k \lambda} \Delta\gamma_{ext} \qquad (3.6)$$

By inserting the values listed in Table 3.1, the chirping-voltage rate was calculated to approximately 6.95 MHz/V.

3. Stability of the diode laser - linewidth of the diode laser system

The linewidth of the diode laser system was checked by the spectral hole-burning technique. The hole width and position provides us with information on the laser frequency stability. The single-mode diode laser was first tuned to the YAG:Tm^{3+} transition line at 7931.50 Å and irradiated the storage crystal, which was mounted in the cryostat and held at a temperature of about 4°K, for several tens of microseconds. The population distribution then changes as some of the atoms in the ground state resonant with the radiated frequency are transferred to the excited state. As the previous irradiation has stopped for a few microseconds the storage crystal is again irradiated. Now by a beam that is tuned in frequency across the previously radiated frequency, a spectral hole will then appear in the transmission spectra due to a weaker absorption at the previously- radiated frequency. The experimental set-up is similar to Figure 3.1 except that only one AOM was involved in the set-up and a photo diode was employed behind the cryostat for detection instead of a PMT. The transmission spectra were recorded by single-shot measurement. Both the amplitude and frequency modulation of the laser beam was controlled by the AOM in the experiment. An on/off modulation voltage to an AOM creates pulses and a voltage ramp applied to the AOM driver scans the frequency. The amplitude and frequency of the two pulses versus time and the data recorded are illustrated in Figure 3.4 (a) and (b). The linewidth of the laser system as a function of burning time was plotted in Figure 3.5.

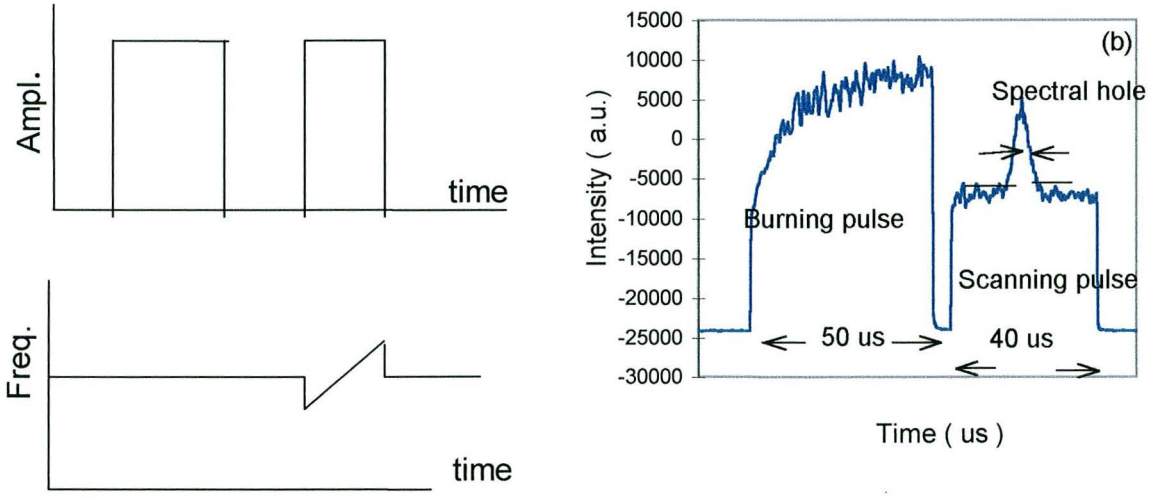

Figure 3.4 (a) Intensity and frequency in the spectral hole burning measurement as a function of time (b) Experimental data illustrating the spectral hole burning measurement

In the experiment data was obtained by measuring the FWHM of the hole as a function of the burning times 10μs, 20μs, 40μs, 100μs, 150μs, and 200μs. The line width of the laser system is given by

$$2\Delta\gamma_{laser} \approx \Delta\gamma_{hole}$$

where $\Delta\gamma_{laser}$ and $\Delta\gamma_{hole}$ represent the line width of the diode laser and the width of the spectral hole, respectively. In Figure 3.5 the line width of the diode laser system is plotted versus burning time and shows that the line width of the diode laser system is limited to 350 kHz over a time scale of 200 microseconds.

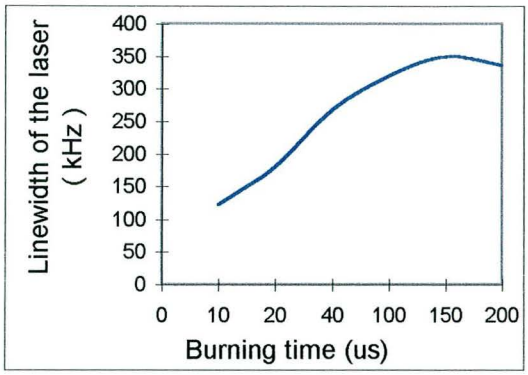

Figure 3.5 Laser line width determined by spectral hole burning as a function of burning time

3.4 The processing crystal, YAG:Tm^{3+}

Several inorganic materials doped with rare earth ions have been used to demonstrate various aspects of optical data storage and processing using spectral hole-burning and photon echo techniques. These materials include YAG, $YalO_3$, LaF_3 and Y_2SiO_5 doped with Pr^{3+}, Eu^{3+}, Tm^{3+} and Er^{3+}, details description is given in Ref. [7]. These materials all have very long dephasing time at low temperature, which means that the homogeneous line width of these materials is narrow at low temperature. They have a high value of the inhomogeneous-homogeneous linewidth ratio (values of 10^6 or higher have been observed). The trivalent rare earth ion thulium doped in YAG and LaF_3 crystals has two advantages relative to several other rare earth ions. One such advantage is that the $^3H_4$ and $^3H_6$ transition line of Tm^{3+} is in the range 790 nm to 797 nm where GaAlAs diode lasers are available. The second advantage is that since Tm has a nuclear spin I = 1/2, there are no zero-field hyperfine splittings that othervise contribute to a complicated pattern of sideholes and antiholes and which leads to a modulated photon-echo decay in the case of short-pulse excitation. The material we used in the experiment is a Yttrium-Aluminium-Garnet (YAG) crystal doped with the trivalent rare earth ion thulium. This crystal is 5 mm thick in the direction of light propagation and has a Tm concentration of 0.1 at %. The chemical formula of YAG is $Y_3Al_5O_{12}$[15]. The structure of YAG is cubic and the lattice is 12.01 Å. The trivalent thulium ions replace trivalent yttrium ions in sites of D_2 symmetry [8,15]. The lower energy levels of the trivalent thulium ions in

YAG include the $^3H_4$ and $^3H_6$ states. Between these two states the absorption line is at 793.1 nm with a homogeneous linewidth and an inhomogeneous linewidth of a few kilohertz and a few tens of gigahertz, respectively. The absorption of this YAG:Tm^{3+} crystal at liquid helium temperature was observed by measuring the transmission intensity. The absorption is here defined as

$$\alpha = (I - I_{transmission})/I \qquad (3.7)$$

where I is the intensity of the incidence light, $I_{transmission}$ is the intensity of the transmitted light. The absorption saturated in about 10 microseconds at a laser output power of 30 mW. The absorption varies as a function of the wavelength of the radiation. Figure 3.6 plots a curve of the absorption versus wavelength.

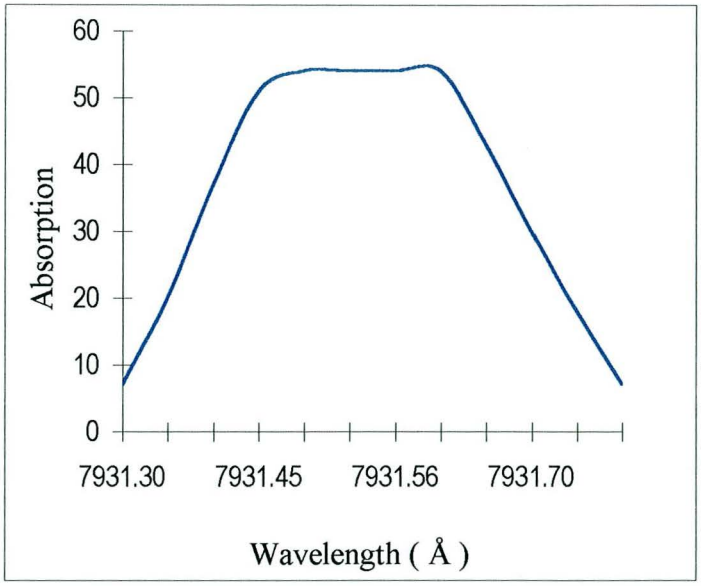

Figure 3.6 The absorption of YAG:Tm^{3+} as function of the wavelength

The figure shows that the maximum absorption is 54% within the interval 7931.50 Å to 7931.60 Å. The full width of half maximum of the absorption is about 0.35 Å in the range from 7931.35 Å to the 5931.70 Å, which corresponds to a value of 19 GHz.

In following sections optical data compression in YAG:Tm^{3+} using the external-cavity diode laser [3] equipped with an intra-cavity electro-optical crystal will be described.

4. Experimental results and discussion

4.1 Single pulse compression

Single pulse compression can be performed using the two pulse photon echo method. A pulse, referred to as the first pulse, with a linear frequency chirp and a duration T_1 is compressed by a compression pulse, referred to as the second pulse with length of $T_2=T_1/2$. The compression is achieved by frequency chirping the second pulse twice as fast as the first pulse. A RF signal with an on/off sequence controlled by a pulse generator, or a personal computer with built in delay generator cards, generates pulses to the pair of AOMs shown in the experimental setup in Figure 3.1. Two pulses are then diffracted towards the crystal when the continuous wave beam from the diode laser passes through the AOMs. The frequency chirps are generated by applying a voltage ramp from a function generator to the diode laser system intra-cavity EOC. There is a linear relation between the chirps and the voltage ramp as indicated in section 3.3.2. The amplitude and frequency of the pulse sequence versus time is illustrated in Figure 4.1, where also the echo signal has been indicated.

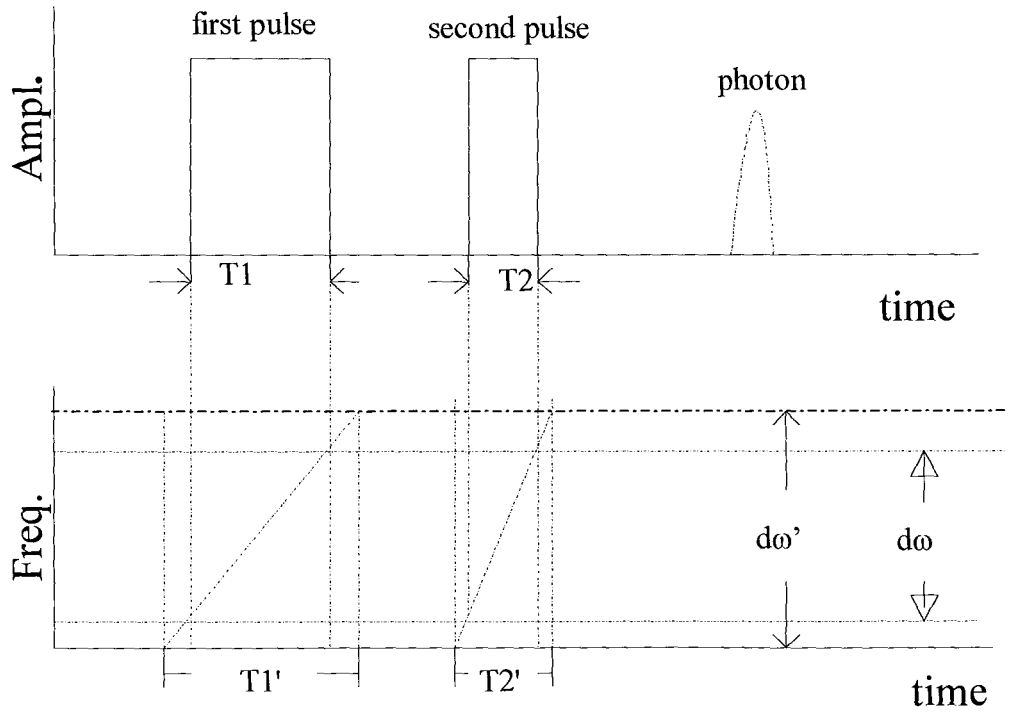

Figure 4.1 Amplitude and frequency of the two pulse sequence as well as the two pulse photon echo signal

As shown in Figure 4.1, T_1 and T_2 are the length of the first pulse and second pulse respectively. Both pulses are chirped over the same frequency interval, which means that the chirping speed of the second pulse is faster than that of the first one. T_1' and T_2' represent the time that is needed for the frequency to be chirped over interval dω'.

Here the relationship between T_1' and T_2' is T_1'=2T_2', so that the chirping rate of the first pulse and second pulse can be expressed as $R_1 = \frac{d\omega'}{T_1'}$ and $R_2 = \frac{d\omega'}{T_2'}$, respectively. This gives $2R_1 = R_2$ and therefore, the chirping intervals of the two pulse is given by

$$d\omega = T_1 \frac{d\omega'}{T_1'} = T_2 \frac{d\omega'}{T_2'},$$

where dω' is defined as the total chirping interval during time intervals T_1' and T_2'.

The sample irradiated by the two excitation pulses is submerged in liquid helium in the cryostat. The emitted echo is detected by a photo multiplier tube (PMT). An additional AOM is inserted between the crystal and the PMT to prevent the excitation pulse from entering the PMT. The PMT signal recorded on the oscilloscope is transferred to the computer for further analysis. The experimental schematic is as shown in Figure 3.1.

In the single pulse compression experiment T_1 was chosen to of 10 μs, 20μs and 30μs and the corresponding T_2 to 5 μs, 10 μs and 15 μs. Figure 4.2 (a) and (b) are typical experimental data detected in the single pulse compression. By analysing measurement data the duration (full width of half maximum) of the echo signal and the intensity of the echo signal can be determined for different pulse durations and chirping rates.

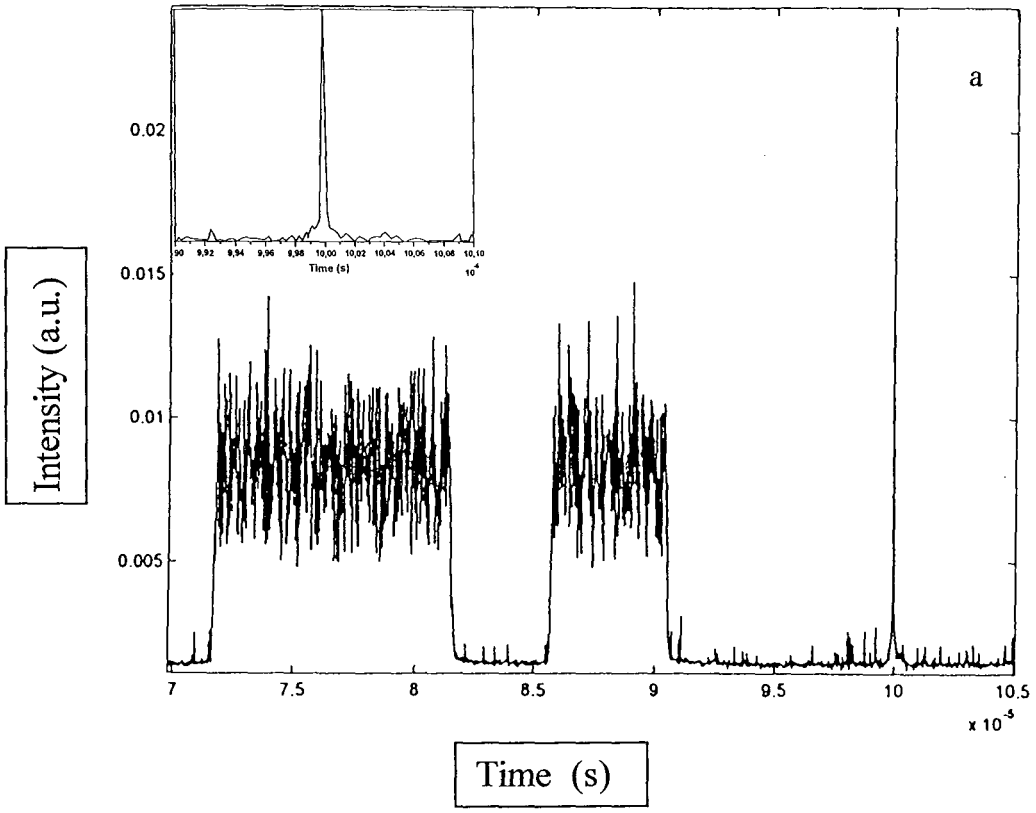

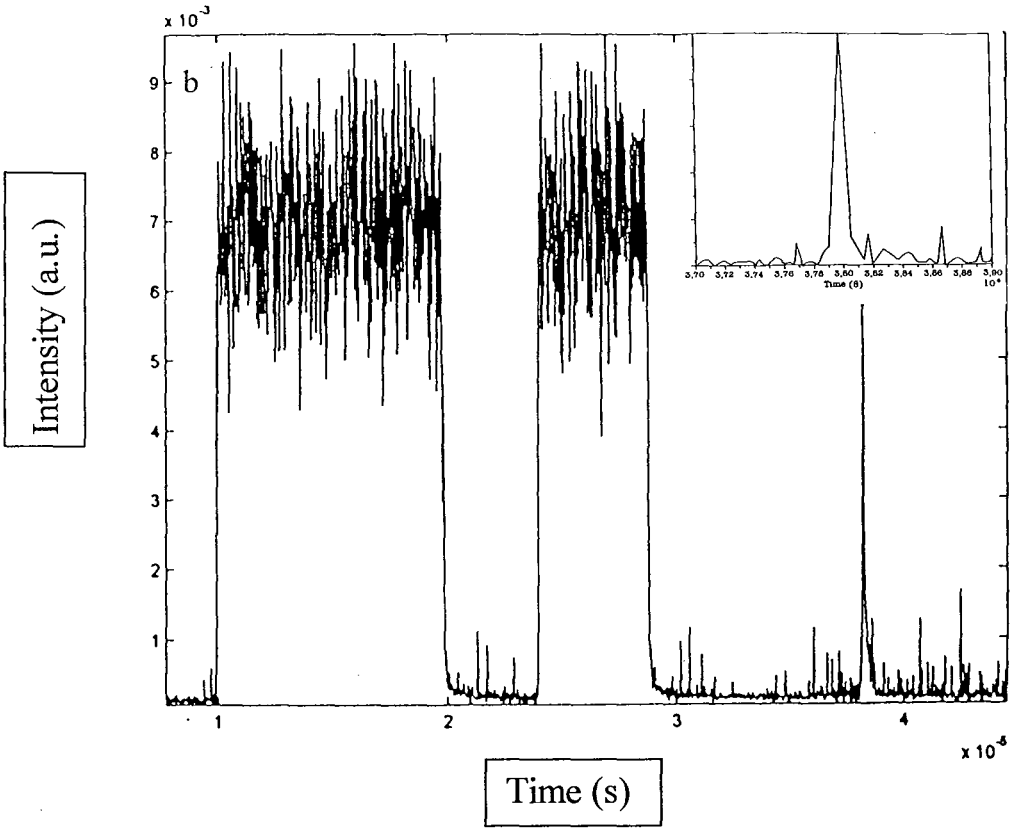

Figure 4.2 Experimental data on single pulse compression. The insets are expanded views of the echo signal. (a) Single-shot measurement, T_1=10μs, dω=230MHz (b) Data recorded by averaging over 7 shots, T_1=10μs, dω=230MHz.

The first pulse and second pulse in Figure 4.2 (a) and (b) have a duration of 10 μs and 5 μs, respectively. The chirping intervals over these two pulses are about 230 MHz. The curve (a) in Figure 4.2 is obtained by single-shot measurement and the curve (b) in Figure 4.2 is recorded by averaging over 7 shots. The duration of the photon echo is determined as 69 nanoseconds and 22 nanoseconds related to the curves (a) and (b) in Figure 4.2, respectively. An expansion of the photon echo signals are also shown in each figure.

The single-shot measurement demonstrate that our experimental system is capable to compress a single pulse by a factor of about 500 from a few tens of microseconds to some tens of nanoseconds. But comparing (a) and (b) in Figure 4.2 the duration of the echo in the averaging mode is three times as long as in the single-shot measurement. This indicates that some defects exist in the system, such as time jitter of electronics in the system or phase and frequency fluctuations of the laser beam.

The duration of the single pulse photon echo compression as a function of the pulse chirping intervals is plotted in Figure 4.3 (a), (b) and (c). Figure 4.4 (a), (b) and (c) are the results on the relationship between the intensity of the single pulse compression photon echo and the chirping intervals. In both Figure 4.3 and Figure 4.4 curve (a), (b) and (c) echo signals are recorded by averaging over 7, 12, and 10 shots. The pulse lengths have been chosen to (a) $T_1 = 2T_2 = 10$ μs; (b) $T_1 = 2T_2 = 20$ μs and (c) $T_1 = T_2 = 30$ μs.

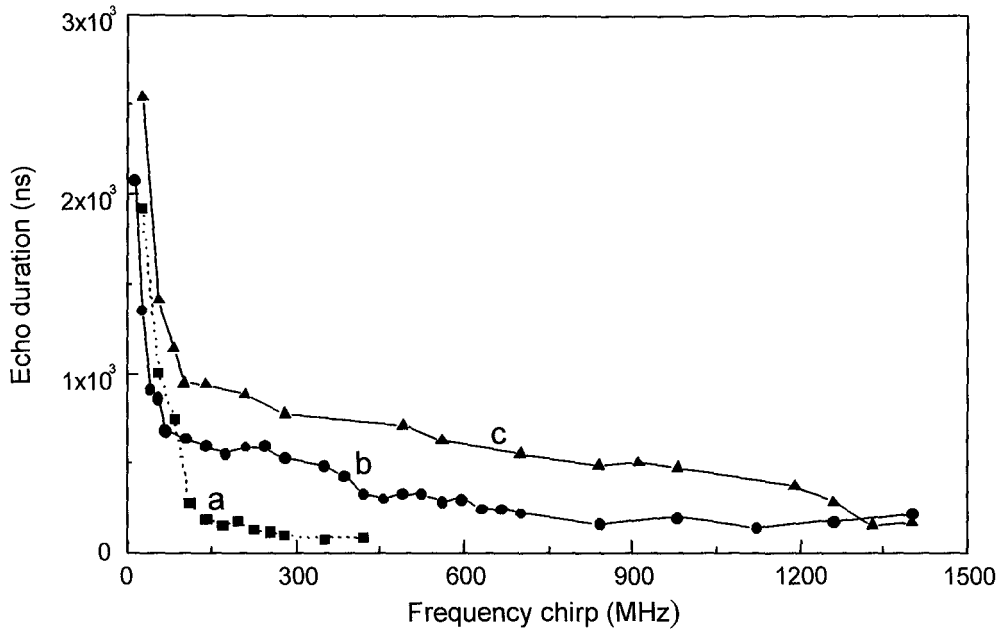

Figure 4.3 Duration of single pulse compression as functions of the frequency chirping intervals. (a) $T_1=2T_2=10\mu s$; (b) $T_1=2T_2=20\mu s$; (c) $T_1=2T_2=30\mu s$.

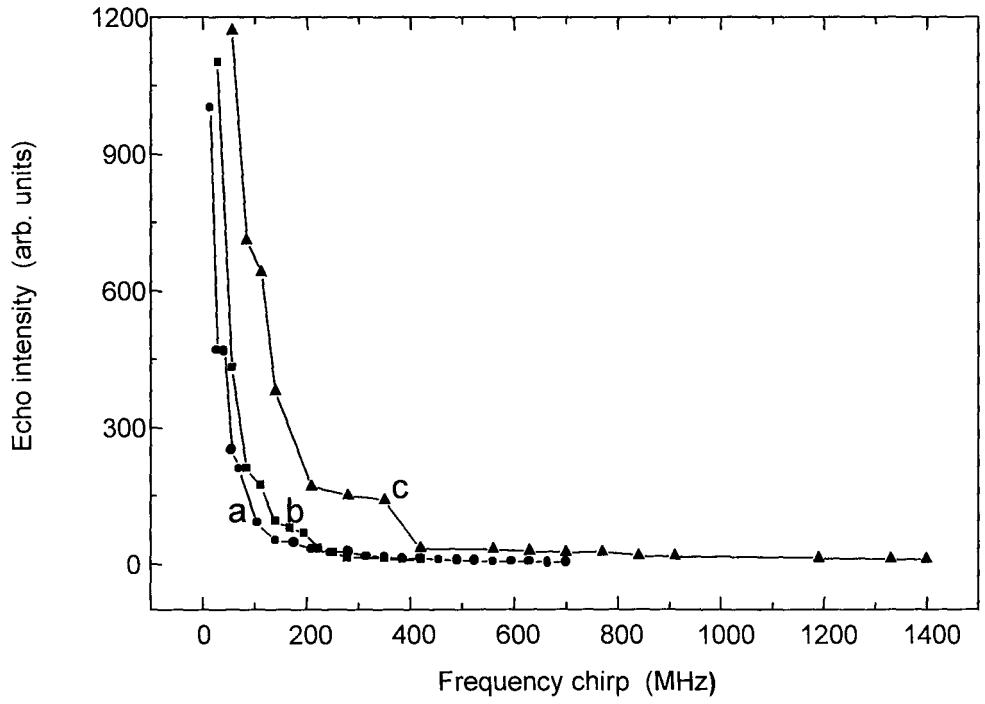

Figure 4.4 Intensity of single pulse compression photon echo as function of pulse frequency chirping intervals.
(a) $T_1=2T_2=10\mu s$; (b) $T_1=2T_2=20\mu s$; (c) $T_1=2T_2=30\mu s$.

The curves (a), (b) and (c) in Figure 4.3 reveals that the duration of the single pulse compression photon echo essentially decreases inversely with increasing frequency chirp interval as predicted by Eq. (2.10). Experimentally it turned out that for very strong compression and/or very large frequency chirps other things than the chirp range limited the minimum pulse duration that could be obtained. We believe these limitations are set by the laser system and the electronics in the setup. By using the homemade external cavity diode laser equipped with the intra-cavity electro-optic crystal and the YAG:Tm^{3+} storage crystal the best single pulse compression achieved was about 500 where a pulse with a duration of a few microseconds was compressed to a few nanoseconds.

The curves (a), (b) and (c) in Figure 4.4 indicated that the intensity of the single pulse photon echo compression decreases inversely with increasing frequency chirping interval. The explanation of this behaviour is that with increasing chirping interval during a fixed time, which means with increasing chirp rate, the number of atoms excited within a fixed frequency interval will decrease. The smaller number of excited atoms after two excitation pulses results in a weaker signal intensity. Similarly, comparing (a), (b) and (c) longer pulse duration results in higher intensity of the echo signal at constant frequency chirping interval, because of the larger number of the atoms excited after two excitation pulses.

4.2 Multi-bit pulse train compression

From what has been written previously it is reasonable to predict that an arbitrary pulse train can be compressed by chirping the total pulse train and the compressing pulse. The duration of the echo signal can be estimated in a way analogous to the single pulse compression and with similar methods as the single pulse compression. The scheme is illustrated in Figure 4.5. At the top of the figure the pulse sequences are shown. The pulse train has a total length of T_1. It is composed of N bits. Each bit has a pulse length of T_b and a bit center-to-center separation of T_s. The compressing pulse which is also denoted the second pulse has length T_2. The relationship between the T_1 and T_2 is given by $T_1 = 2T_2$. The lower part of the figure shows the frequency chirping sequence of the pulse and the pulse train. The pulse train and the second pulse are chirped over same frequency interval, $d\omega'$, within the times T_1' and T_2', where $T_1' = 2T_2'$. As the two pulses are chirped over the same frequency intervals the frequency chirping rate of the second pulse is twice as fast as that of the pulse train.

As expressed by equation (2.20) in the theory section 2.2.2, the envelope of a multi-bit pulse train compressed by a photon echo will have the same shape as that of a single compressed pulse. In the multi-bit pulse train compression experiments, 5, 7, 10, 16 and 20 -bits pulse train compression were demonstrated. A photo multiplier tube (PMT) was employed for measuring the duration of the compressed multi-bit pulse train. The photon echo signal was averaged over 10 shots, and the data was transferred to the computer.

Figure 4.6 (a) shows a typical example of the photon echo multi-bit compression. In this figure number of bits is 10, each bit has a length of 1.34 μs, the center-to-center separation of two bits is 2.19 μs, the chirping rate is about 770MHz/21.4μs, so the chirping interval over the multi-bit pulse train and the second pulse each are about 650 MHz. The photon echo signal was determined to have duration (FWHM) of 212 nanoseconds. Compressing a 10-bits pulse train with a total length of 20 μs to the 212 nanoseconds gives compression factor of 92.

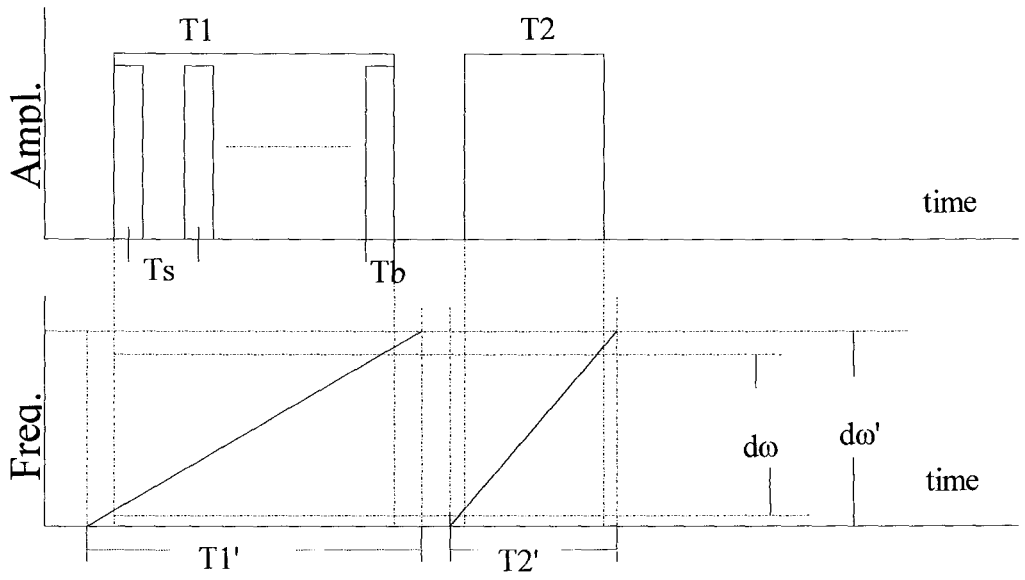

Figure 4.5 Amplitude (a) and frequency (b) chirp in a multi-bit pulse train compression experiment

Figure 4.6 (b) shows a 20-bit pulse train compression with 30 μs duration. In this figure T_b = 0.77 μs, T_s = 0.68 μs, the chirping rate $2R_1 = R_2 = d\omega'/T_1' =$ 770MHz/31.4μs, so the chirping intervals during T_1 and T_2 is approximately 735 MHz. The duration of the photon echo is measured as 370 ns, which gives a compression factor of 80. Figure 4.6 (a) is the best result for the multi-bit pulse train compression and demonstrates a compression factor of almost 100. Figure 4.6 (b) shows the highest number of the bits that were used in the compression experiments during this work. But neither in Figure 4.6 (a) nor in Figure 4.6 (b) the multi-bit pulse train compression shows the side-bands within the envelope of the photon echo signal which should be present according to equation (2.12) in the theoretical section. This leads us to check whether the full information in the many bit pulse train really was retained during the multi-bit compression. Therefore 3, 5, 7, and 10 bit pulse compression were performed and measured by single shot measurements. Figure 4.7 (a), (b), (c), and (d) shows the experimental data together with the theoretical data from equation (2.12). In Figure 4.7 the experimental data basically is consistent with theory even if the signal-to-noise not is sufficiently good that all information is retained. In the single-shot mode used in the recordings displayed in Fig 4.7 the strongest side bands are clearly visible.

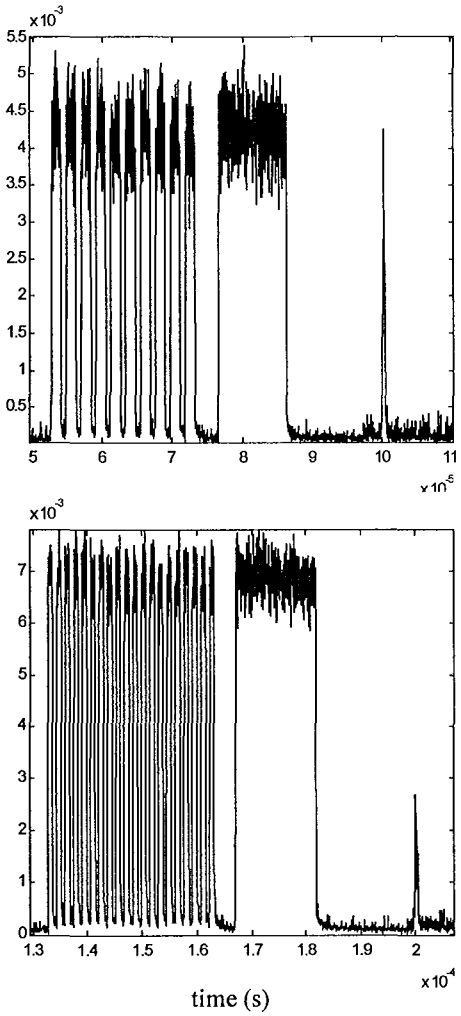

Figure 4.6 Data from photon echo multi-bit pulse compression.
(a) 10-bit photon echo pulse compression. The multi-bit pulse train length (T_1) is 20μs, the photon echo duration (T_e) is 212ns;
(b) 20-bit photon echo pulse compression. The multi-bit pulse train length (T_1) is 30μs, the photon echo duration (T_e) is 371ns.

In averaging mode time jitter between the trigger signal to the oscilloscope and the frequency chirp broaden the echo peak and washes out the side band structure similar to what was the case in averaging mode in the single pulse compression.

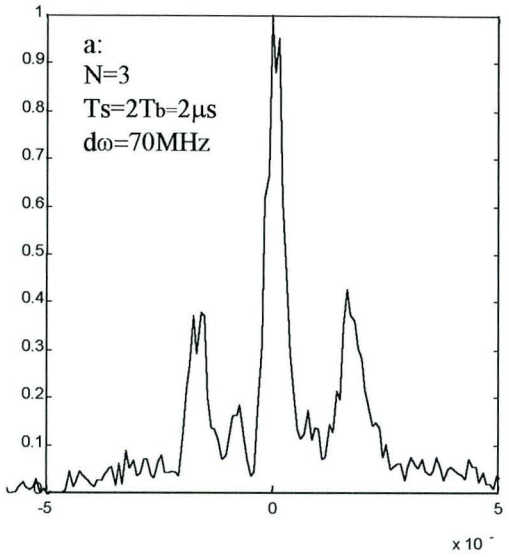
a:
N=3
Ts=2Tb=2μs
dω=70MHz

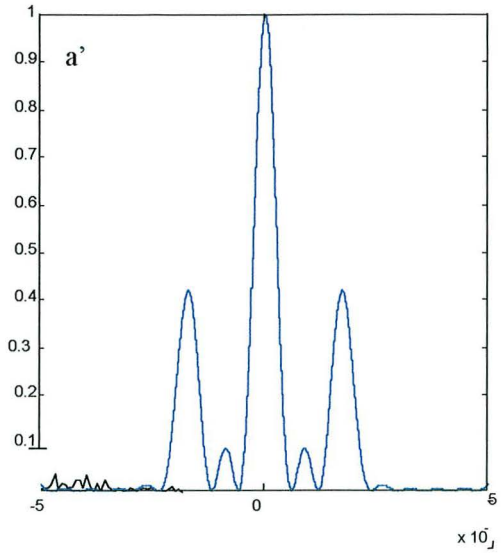
a'

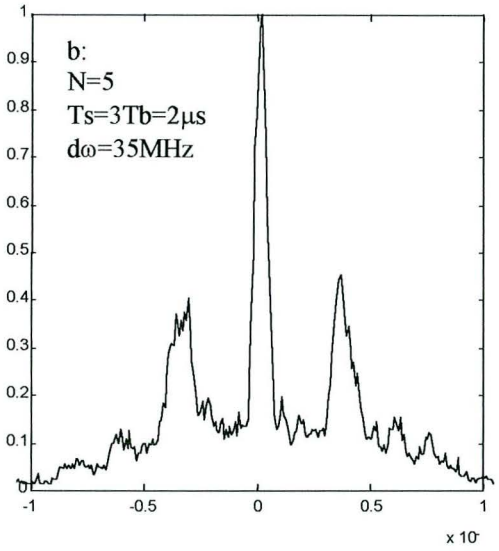
b:
N=5
Ts=3Tb=2μs
dω=35MHz

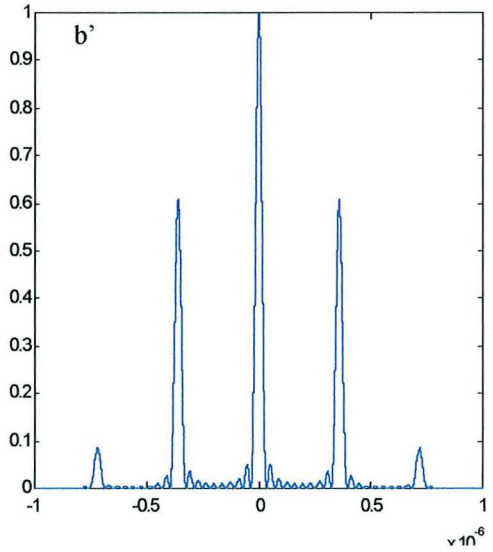
b'

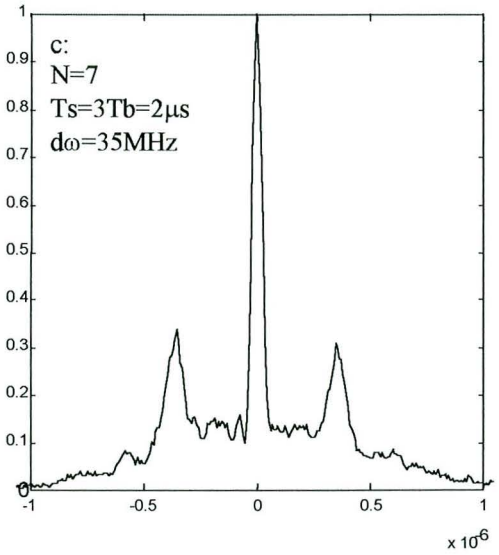
c:
N=7
Ts=3Tb=2μs
dω=35MHz

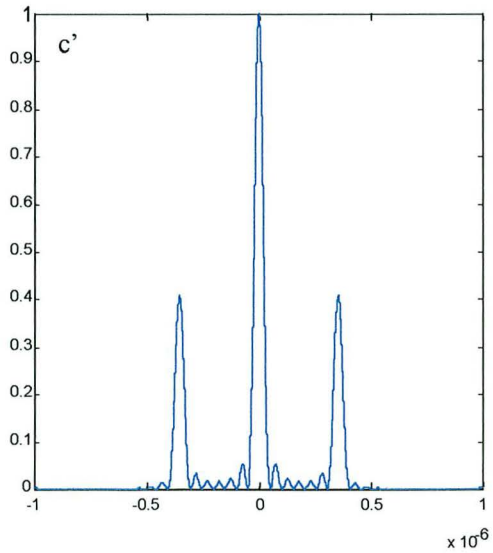
c'

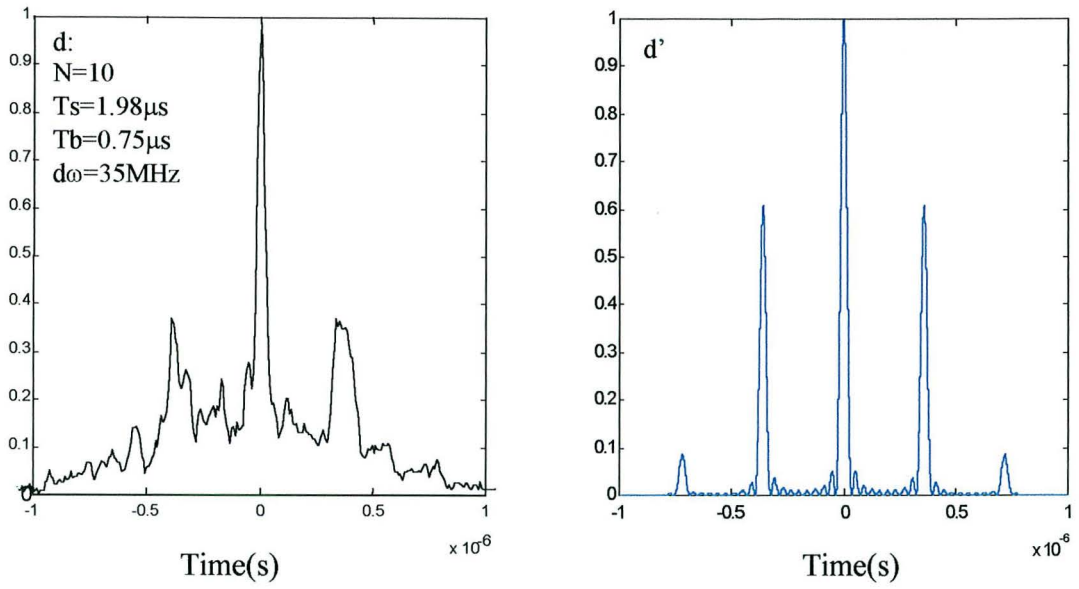

Figure 4.7 Experimental and theoretical data on multi-bit pulse train compression, The left-hand of the figure are obtained by experiment, all parameters are showed in the left top of experimental data. In the figure N is the number of bits. T_s and T_b stand for bit-bit center separation and one bit length, respectively. The frequency chirping is over dω within time of 21.4μs. The right hand figure is obtained by inserting corresponding the parameters in Eq. 2.20. The peak intensity has been normalised to unity.

Finally the relationship between the duration of the multi-bit pulse trains and the frequency chirp is investigated. Figure 4.8 (a) and (b) show the duration of the photon echo from the 10-bit pulse train and 20-bit pulse train compression as function of the chirping interval, respectively. T_b = 1.34 μs, T_s = 0.85 μs, T_1 =2T_2 = 20 μs, T_1' =2T_2' = 21.4 μs in Figure 4.8 (a), T_b = 0.771 μs, T_s = 0.679 μs, T_1 =2T_2 = 30 μs, T_1' =2T_2' = 31.4 μs in Figure 4.8 (b). From the curve in both Figure 4.8 (a) and (b) it is indicated that the duration of multi-bit pulse train compression decrease with increasing chirping intervals. Comparing the Figure 4.3 and Figure 4.8 on the echo duration for single pulse compression and multi-bit pulse train compression as a function of the frequency chirping interval, it is clear that both single pulse and multi-bit pulse train compression follow the same tendency, as they also should be from theory. The duration of multi-bit pulse train photon echo is longer than that of single pulse photon echo as they have same length and with same frequency chirping interval.

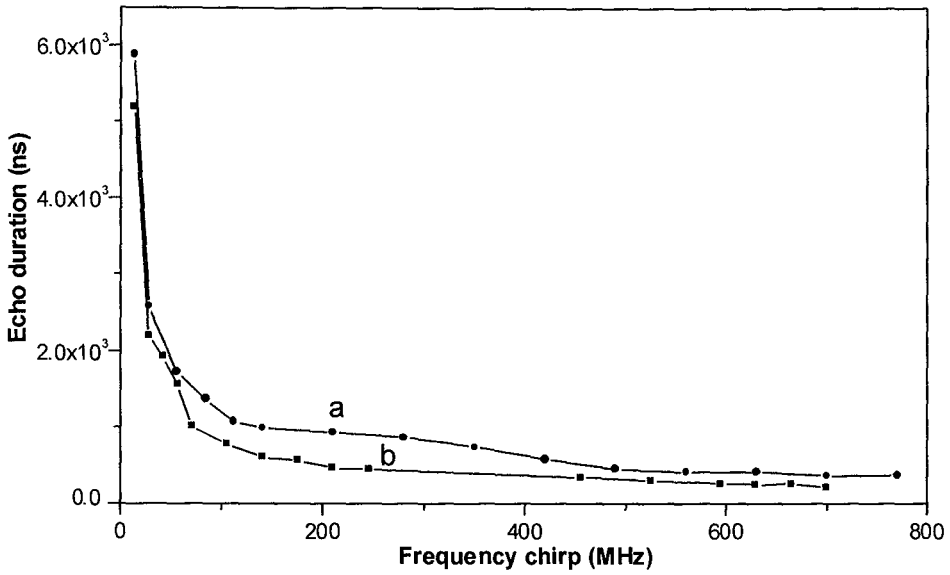

Figure 4.8 The echo duration in multi-bit pulse train compression as a function of the frequency chirp over the pulse train, in (a) number of bits N=10, one bit pulse length T_b=1.34μs, bit-bit centre separation T_s=2.19μs, frequency chirping rate R=700MHz/21.4μs; in (b) N=20, T_b=0.771μs, Ts=1.45μs and R=770MHz/31.4μs.

4.3 Observation of the duality of space and time as manifested in photon echo pulse compression

The other interesting phenomenon, duality between space and time, were observed during the photon echo processing experiments. The equivalence between the time and space domains in this work can be seen by comparing the echo signal in time with the multi-slit diffraction in space in the Fraunhofer approximation. The demonstration also supplies a way to further explore the space-time duality in photon echoes.

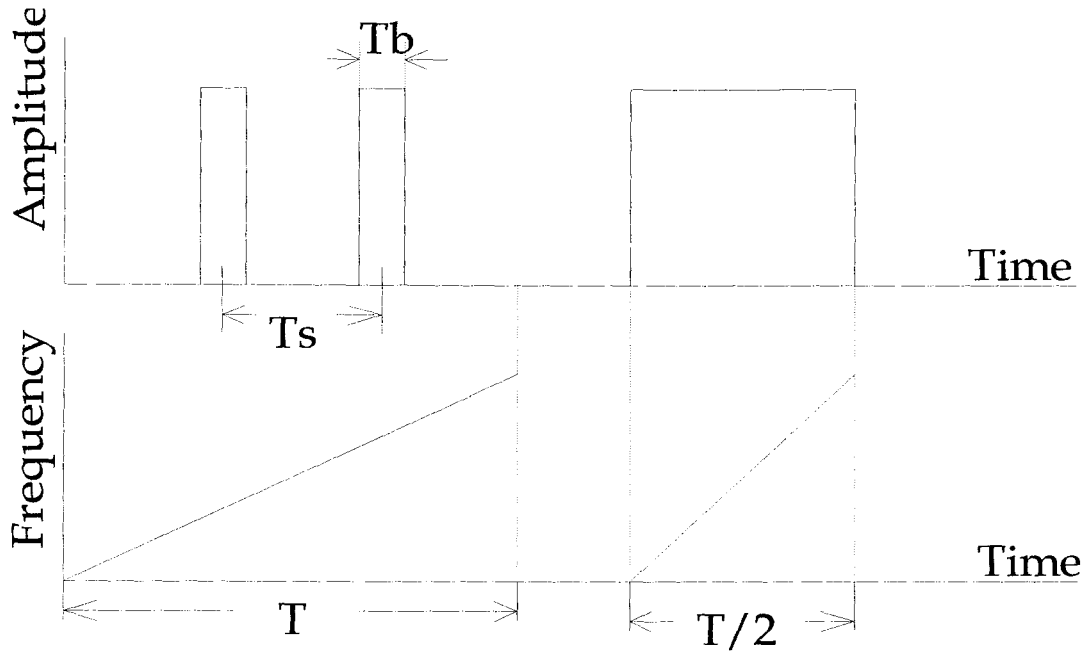

Figure 4.9 Amplitude and frequency sequence of two-pulse for interference

The experiment was designed as illustrated in Figure 4.9. Two bits with identical lengths (T_b) of 1μs with bit-to-bit centre separation (T_s) of 2μs, 3μs, 4μs and 8μs were used. This means that the bit-to-bit centre separation T_s is 2, 3, 4, and 8 times as large as the bit-pulse length T_b. The compressed two-bit pulse was recorded by single-shot measurement as the frequency chirping rate over the two-bit pulses was 7 MHz, 14 MHz, 21 MHz, and 35 MHz within a time of 14 μs. Figure 4.10 shows typical data obtained in the experiment, (a) and (b) are the photon echo signal where $T_s=2T_b=2\mu s$ and a frequency chirping interval of 7MHz and 14 MHz over approximately 14 μs, (c) is the photon echo signal with $T_s=3T_b=3\mu s$ and a frequency chirping interval of 7 MHz over approximately 14 μs. From this figure the side-band can be identified clearly within the envelope of the photon echo signal. As can be seen from figures (a) and (b), the peak-to-peak separation becomes short as the chirping intervals increase. This corresponds that if keeping identical slit width, the diffraction pattern will become dense as increment in focal length of the lens inserted between the slit and the screen. The frequency chirping is equivalent of the lens. From (a) and (c) it is shown that the peak-peak separation decreases with increasing the bit-bit centre separation, the peak-peak separation of photon echo is 0.73 μs and 0.54 μs in the case (a) and (c) respectively. One can easy to understand the duality of time and space by comparing equation (2.12) to the description of Fraunhofer diffraction in the classical optics, the mathematical formulation is exactly analogous for these two cases. Figure 4.10 (a'), (b') and (c') show the theoretical curve defined by the equation (2.12) which correspond to the experimental data (a), (b) and (c).

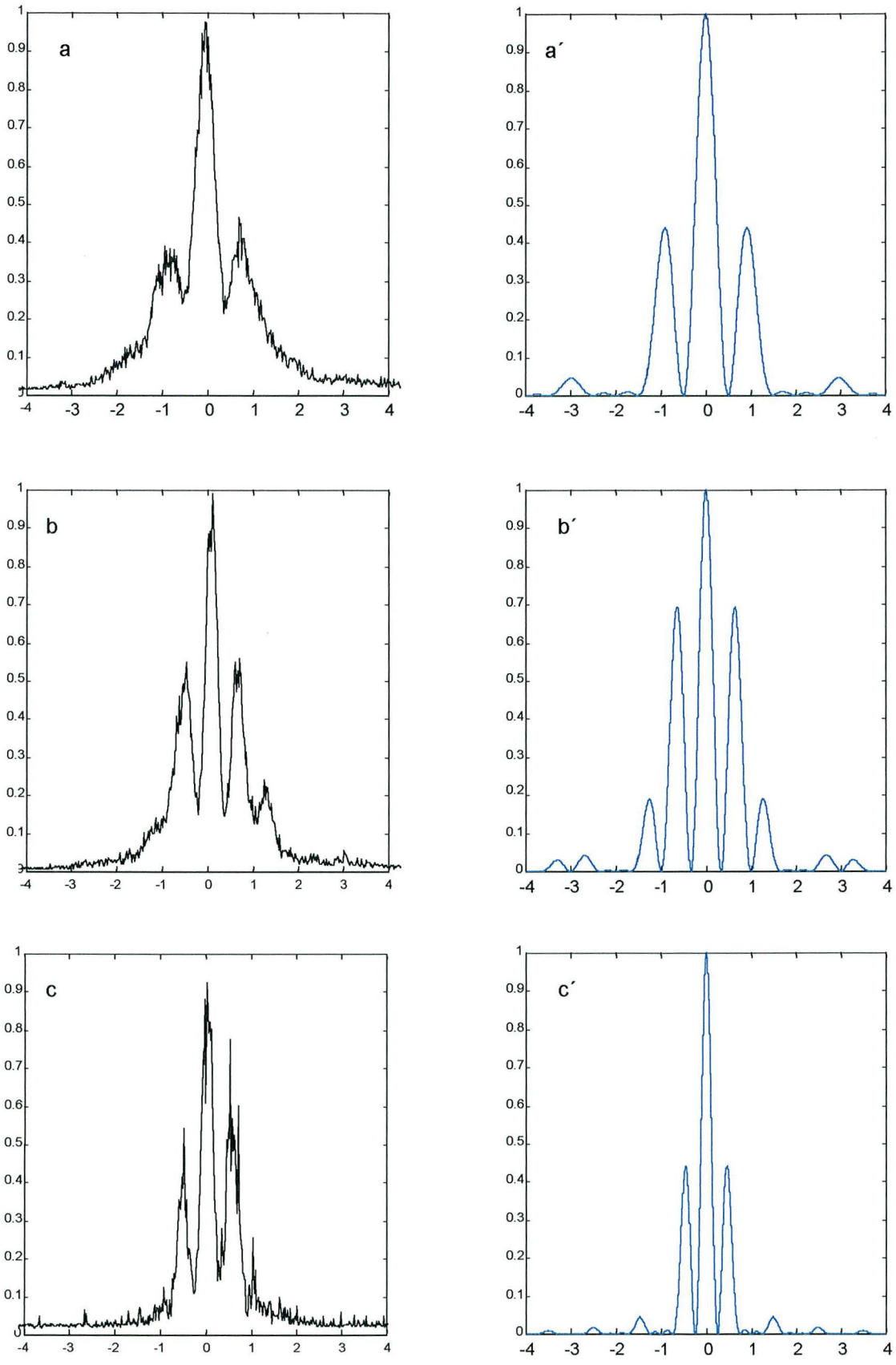

Figure 4.10 Time domain diffraction pattern of two-pulse photon echo compression

5. Conclusion

Based on the results in this work, the following conclusion can be made:

1. Laser system

The diode laser is a very convenient piece of equipment. The optical data storage using photon echo technique can be carried out with diode lasers and by using e.g. the storage material YAG:Tm^{3+}. Diode lasers in general have a large attractive potential in the future applications because of their simplicity, high quantum efficiency, low cost, compact size, and their frequency tunability in the infrared region. The properties of the external cavity diode laser system equipped with the intra-cavity electro-optic crystal were investigated. The frequency tunability can be achieved by adjusting the diffraction grating, temperature and operation current of the external cavity diode laser, linear frequency chirps can be obtained by supplying a voltage ramp to the intra-cavity crystal. The diode laser system has a line width of approximately 350 kHz over a time scale of 200 μs. This line width was determined by spectral hole- burning. The frequency chirp is a linear function of the voltage across the EOM and equals 7 MHz/V over large intervals.

2. Storage material - YAG:Tm^{3+} crystal

The photon echo compression was performed at low temperature. The absorption that is an important relevant property for the photon echo compression was checked. The maximum absorption of the YAG:Tm^{3+} crystal was about 40%. The peak absorption occurs between 7931.50 Å and 7931.60 Å with a full width of half maximum of 3.5 Å, which corresponds to 19 GHz.

3. Single pulse and multi-bit pulse train compression

Single pulse and multi-bit pulse train compression were investigated. For both single pulse compression and multi-bit pulse train compression, the duration and intensity of the photon echo signal decrease with increasing frequency chirp during the pulse or pulse train. Single pulse compression by a factor of 454 from 10 microseconds to 22 nanoseconds was demonstrated. A 10-bits pulses train with a length of 20 microseconds was compressed to 212 nanoseconds, which corresponds to a factor of 92 in compression. Both these two values are an order magnitude better than what has been obtained previously in photon-echo compression.

4. Observation of duality of time and space

An interesting phenomenon was observed in the photon echo compression experiments. Several aspects of multi-bit pulse train compression in the time domain were clearly analogous with the behavior of the far field multiple slit diffraction in the Fraunhofer approximation in space. It was demonstrated that if the bit length, bit-to-bit center separation and time in the multi-bit pulse train compression are exchanged against to the slit width, slit-to-slit center separation and wave vector perpendicular to the slits, the mathematical expression describing the multiple pulse train compression photon echo signal in time and the far field multi-bit slit diffraction due to Fraunhofer approximation are the same. This can be helpful to further understand and study the analogy of time in photon echo experiments and diffraction in space and it opens a way to explore space-time duality.

5. Looking into the future

The present photon echo compression results demonstrate an order of magnitude in improvement compared what has been published previously. However, improvements on several aspects, such as higher power, better stability of the laser system, further understanding and theoretical simulation, will make it possible to reach even better compression. An interesting range would be to work in the gap between high-speed electronics and photonics and to compress pulse from the nanosecond region to the picosecond region. By using the diode laser system it is also interesting to demonstrate echo signal decompression experimentally and to find a suitable amplifier and to perform echo signal amplification, regeneration and echo erasure to complete all-optical data storage and processing in the time domain.

6. References

1 B. Boggs, C. Greiner, T. Wang, H. Lin, and T. W. Mossberg, Simple high-coherence rapidly tuneable external-cavity diode laser, Optics Letters, Vol. 23, No. 24, 1906-1908 December 15,1998.

2 C. Greiner, B. Boggs, T. Wang and T. W. Mossberg, Laser frequency stabilisation by means of optical self-heterodyne beat-frequency control, Optics Letters, Vol. 23, No. 16, 1280-1282 august 15,1986.

3 René Nilsson, Konstruktion och test av en externkavitetsdiodlaser med snabb frekvensavstämning, Examensarbete LRAP-241, LUND, DEC.1998.

4 J. C. Comparo, The diode laser in atomic physics, Comtemp. Phys. Vol. 26, No. 5, 443-477, 1985.

5 Zhu et al., Continuous coherent trasient optical processing in a solid, Opt. Lett. 20, 2514 (1995).

6 Shen et al., Time-domain optical memory of image storage and high-speed image processing, Appl. Opt. 32, 5810 (1993).

7 Baozhu Luo, Optical memories and processing in time- and frequency domain Ph. D thesis, Lund reports on Atomic Physics, LRAP-233, Lund University, June, 1998.

8 Y. S. Bai, H. Lin, and T. W. Mossberg. Optical bit-rate conversion and bit-stream time reversal by the use of swept-carrier frequency-selective optical data storage techniques, Optics Letters, Vol. 20, No. 19, 2033-3035, October 1,1986.

9 Y. S. Bai, and T. W. Mossberg. Experimental studies of photon-echo pulse compression, Optics Letters, Vol. 11, No. 1, 30-32, January 1986.

10 Felix R. Graf, Bernd H. Plagemann, Eric S. Maniloff, Stefan B. Altner, Alois Renn, and Urs P. Wild, Data compression in frequency-selective materials using frequency-swept excitation pulses, Optics Letters, Vol. 21, No. 4, 284-286 February 15, 1996.

11 Zeylikovich et al., Terabit speed retrieval of femtosecond accumulated photon echoes, Opt. Lett. 20, 749, (1995).

12 Merkel & Babbitt, Optical coherent transient header/data isolation technique, Optics Letters, Vol. 21, 71, (1996).

13 Coherent transient spectroscopy - Lab instruction for the course Atomic and Molecular spectroscopy, FAF080, Lund Institute of Technology.

14 Sven-Göran Pettersson, Stig Borgström, and Hans Hertz, Advanced optics, Dept. of Physics LTH, 1996.

15 Http://www.bicron.com/13 YAG.htm

16 Elman er al., Photon echo data erasure, amplification of photon echo data and other aspects on photon echo data processing, invited talk, Frontiers of Applications of Photospectral Holeburning, Big Sky, MT, February-97.

17 Maniloff et al., Recording of 6000 holograms by use of spectral hole burning, Appl. Opt. 34, 4140 (1995).

18 Mitsunaga et al., Holofraphyic motion picture by Eu2+: Y2SiO5, Optics Letters, Vol. 19, 752 (1994).

19 Shen & Kachru, Optical header recognition by spectroholographic filtering, Optics Letters, Vol. 20, 2508, (1996).

20 Kröll & Elman, Photon-echo-based logical processing, Opt.Lett.18, 1834 (1993).

21 Elman et al., The influence of laser phase and frequency fluctuations on photon echo data erasure, JOSA B13, 1905 (1996)

22 Babbitt & Mossberg, Quesi-two-demensioal time-domain color memories: process limitations and potentials, JOSA B11,1948 (1994).

23 Kröll &Tidlund, Recording density limit of photon-echo optical storage with high speed writing and reading, Appl. Opt. 32, 7233 (1993).

24 Lin et al., Demonstration of 8- Gbit/in.^{2} areal storage density based on swept-carrier frequency-selective optical memory. Optics Letters 20, 1658 (1995).

7. Acknowledgement

I have had the pleasure to join the active group organised by Prof. Stefan Kröll, where interesting topics and first class research is carried out. I am lucky to have been accepted and that my diploma thesis advisor Prof. Stefan Kröll has giving me the opportunity to work with this project at the research frontier of photon echo processing. Here I start my scientific research work abroad. I would be very proud to recall the experience a few years later or even a few decades later. I have met very kind, nice colleagues, their help, encouraging instructions and discussions have been important and useful. I would like to express my sincere appreciation to Prof. Stefan Kröll, Niklas Ohlsson, Dr. R. Krishna Mohan, Ulf Gustafsson and Mikael Afzelius, as well as to all the friends who have provide a pleasant atmosphere in Lund University.

I very gratefully acknowledge the director of the International Master's Program, Prof. Leif Johansson in Linköping University, for his direction and endless encouragement at the studying and fundamental training period in Linköping and during the diploma work period in Lund.

I appreciate very much the financial support from the STINT scholarship during the International Master's Programs in Sweden.

I thank my husband and my daughter for their solid and strong support, supplying me in the spirit, energy and time. I have been enjoying the wonderful love from them.

I really feel that any words are difficult to fully express my feeling, let me instead reply by my high performance in the future.